Lithos 376–377 (2020) 105763

Contents lists available at ScienceDirect

Lithos

journal homepage: www.elsevier.com/locate/lithos

Research Article

Early Paleozoic intracontinental granites in the Guangzhou region of South China: Partial melting of a metasediment-dominated crustal source

Xiao Liu [a,b], Qiang Wang [a,b,c,*], Lin Ma [a,*], Jin-Hui Yang [d], Guo-Ning Gou [a], Quan Ou [a,e], Jun Wang [a]

[a] State Key Laboratory of Isotope Geochemistry, Guangzhou Institute of Geochemistry, Chinese Academy of Sciences, Guangzhou 510640, China
[b] College of Earth and Planetary Sciences, University of Chinese Academy of Sciences, Beijing 100049, China
[c] CAS Center for Excellence in Tibetan Plateau Earth Sciences, Beijing 100101, China
[d] Institute of Geology and Geophysics, Chinese Academy of Sciences, Beijing 100029, China
[e] State Key Laboratory of Oil and Gas Reservoir Geology and Exploitation, Institute of Sedimentary Geology, Chengdu University of Technology, Chengdu 610059, China

ARTICLE INFO

Article history:
Received 25 April 2020
Received in revised form 29 August 2020
Accepted 31 August 2020
Available online 8 September 2020

Keywords:
Biotite granite
Two-mica granite
Muscovite granite
Baiyunshan and Maofengshan
Intracontinental orogeny
South China

ABSTRACT

Whether the formation of early Paleozoic granites in the South China Block was related to intracontinental orogenic processes or oceanic subduction continues to be debated. Here, we present whole-rock major element, trace element, and Sr—Nd isotopic data, as well as secondary ion mass spectrometry and laser ablation–inductively coupled plasma–mass spectrometry zircon U—Pb geochronological and Hf—O isotopic data, from biotite, two-mica, and muscovite granites in the Baiyunshan and Maofengshan areas of Guangzhou City, South China. Zircon U—Pb ages reveal that these rocks were formed during the early Paleozoic (446–438 Ma). These muscovite- and biotite-bearing granites have high SiO_2 (69.0–80.4 wt%) and K_2O (3.19–5.32 wt%) contents, and low MgO (0.46–1.17 wt%) contents. The granites are enriched in Rb, Th, U, and Pb, and depleted in Ba, Sr, Nb, and Ti. The Baiyunshan muscovite granites and Maofengshan biotite granites are slightly to moderately enriched in light rare-earth elements [LREEs; $(La/Yb)_{CN} = 2.27–15.1$] with slight to pronounced negative Eu anomalies ($Eu/Eu^* = 0.27–0.72$), whereas the Baiyunshan two-mica granites are significantly enriched in LREEs [$(La/Yb)_{CN} = 19.6–32.1$] with moderate negative Eu anomalies ($Eu/Eu^* = 0.42–0.58$). These muscovite- and biotite-bearing granites have enriched whole-rock Nd and zircon Hf isotopic compositions ($\varepsilon_{Nd}(t) = -12.1$ to -7.6; $\varepsilon_{Hf}(t) = -11.4$ to -0.8), and high zircon $\delta^{18}O$ values (8.5‰–10.0‰). We suggest that the Baiyunshan granites were formed by partial melting of metasedimentary rocks, as they contain primary muscovite and have high zircon $\delta^{18}O$ values. The Maofengshan granites were formed by partial melting of a hybridized crustal source containing metasedimentary rocks with subordinate amphibolites, as they have high zircon $\delta^{18}O$ values, variable whole-rock SiO_2 contents, and biotite compositions similar to those crystallized in I- and S-type magmas. These granites, along with the widespread early Paleozoic S-type granites in the Wuyi–Yunkai orogen, are distributed across a broad area rather than in a narrow belt. In addition, early Paleozoic S-type granites in the South China Block generally do not show younging trends from east to west or south to north. Moreover, the Baiyunshan–Maofengshan granites show geochemical characteristics similar to *syn*- or post-collisional granites and different from volcanic arc granites. We therefore propose that these muscovite- and biotite-bearing granites were formed in an intracontinental orogenic setting.

1. Introduction

Orogenic belts can form through subduction and accretion, subduction and collision, or as intracontinental orogenic belts (Cawood et al., 2009). Unlike accretionary and collisional orogens, intracontinental orogenic belts form far from plate boundaries (Pirajno et al., 2009). Intracontinental orogenic belts are closely related to the reactivation of ancient thrust structures or pre-existing lithospheric weak zones, such as the Damara orogen in southwestern Africa (Nex et al., 2001), the Alice Springs orogen in central Australia (Raimondo et al., 2011), the Laramide orogen in western North America (Copeland et al., 2017), the Cenozoic Tianshan orogen in central Asia (Li et al., 2016), and the Pyrenean orogen in western Europe (Choukroune, 1992). The early Paleozoic Wuyi–Yunkai orogen in South China is considered to be an important intracontinental orogen (Li et al., 2010; Shu et al., 2015; Wang et al., 2010). Study of the Wuyi–Yunkai orogen is important

* Corresponding authors at: State Key Laboratory of Isotope Geochemistry, Guangzhou Institute of Geochemistry, Chinese Academy of Sciences, Guangzhou 510640, China.
E-mail addresses: wqiang@gig.ac.cn (Q. Wang), malin@gig.ac.cn (L. Ma).

https://doi.org/10.1016/j.lithos.2020.105763
0024-4937/

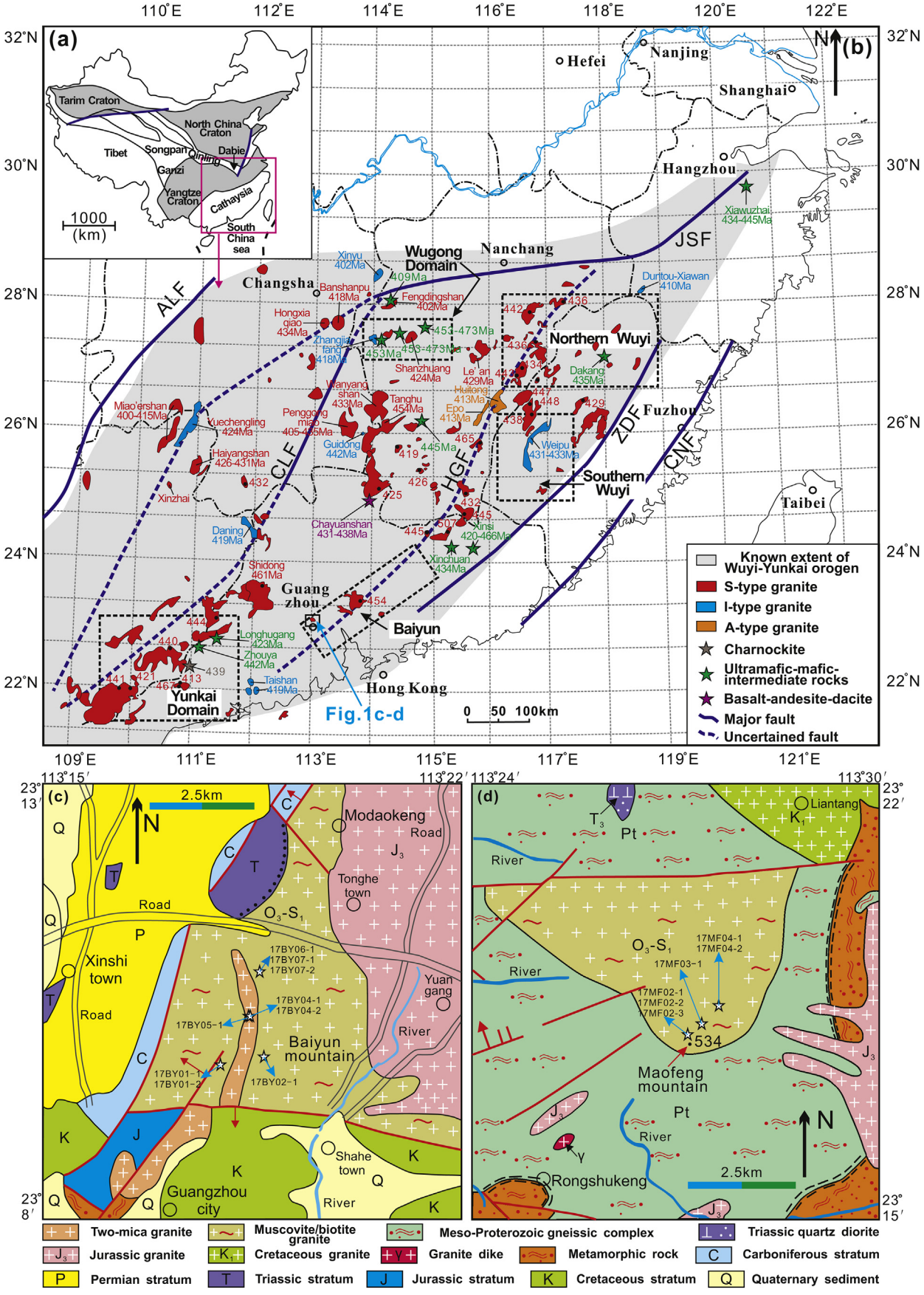
(a)
Tarim Craton
North China Craton
Tibet
Songpan
Qinling
Dabie
Ganzi
Yangtze Craton
Cathaysia
South China sea
1000 (km)
(b)
Hefei
Nanjing
Shanghai
Hangzhou
Xiawuzhai 434-445Ma
Wugong Domain
Nanchang
JSF
Changsha
ALF
Xinyu 402Ma
Banshanpu 418Ma
Fengdingshan 402Ma
409Ma
Durtou-Xiawan 410Ma
Hongxiaqiao 434Ma
Zhangjiafang 418Ma
453-473Ma
Northern Wuyi
Shanzhuang 424Ma
Le'an 429Ma
Dakang 435Ma
Wanyangshan 433Ma
Tanghu 454Ma
Huilong 413Ma
Epo 413Ma
Miao'ershan 400-415Ma
Yuechengling 424Ma
Penggongmiao 405-465Ma
Guidong 442Ma
445Ma
Weipu 431-433Ma
Fuzhou
ZDF
CNF
CLF
HGF
Haiyangshan 426-431Ma
Xinzhai
Southern Wuyi
Taibei
Chayuanshan 431-438Ma
Daning 419Ma
Xinsi 420-466Ma
Xinchuan 434Ma
Shidong 461Ma
Guangzhou
Baiyun
Longhugang 423Ma
Zhouya 442Ma
Taishan 419Ma
Hong Kong
Yunkai Domain
Fig.1c-d
0 50 100km
Known extent of Wuyi-Yunkai orogen
S-type granite
I-type granite
A-type granite
Charnockite
Ultramafic-mafic-intermediate rocks
Basalt-andesite-dacite
Major fault
Uncertained fault
(c)
2.5km
Modaokeng Road
Tonghe town
Xinshi town
Yuan gang
Baiyun mountain
17BY06-1
17BY07-1
17BY07-2
17BY04-1
17BY04-2
17BY05-1
17BY01-1
17BY01-2
17BY02-1
Shahe town
Guangzhou city
River
Road
(d)
Liantang
Maofeng mountain
Rongshukeng
17MF04-1
17MF04-2
17MF03-1
17MF02-1
17MF02-2
17MF02-3
534
Two-mica granite
Muscovite/biotite granite
Meso-Proterozoic gneissic complex
Triassic quartz diorite
Jurassic granite
Cretaceous granite
Granite dike
Metamorphic rock
Carboniferous stratum
Permian stratum
Triassic stratum
Jurassic stratum
Cretaceous stratum
Quaternary sediment

for understanding the formation and evolution of eastern Asia, as well as global geodynamics during the early Paleozoic (Wang et al., 2011b, Wang et al., 2013a). The large volumes of early Paleozoic magmatic rocks found in the Wuyi–Yunkai orogen, including granites, ultramafic, mafic, and intermediate intrusive rocks, and basalts, andesites, and dacites were thought to have been generated either by intracontinental orogenic processes (e.g., intracontinental subduction or thrusting; Faure et al., 2009; Li et al., 2010; Wang et al., 2011b; Zhang et al., 2012; Wang et al., 2013a; Shu et al., 2015), or by lithospheric delamination or extension following an intracontinental orogeny (Feng et al., 2014; Huang et al., 2013; Xia et al., 2014; Yao et al., 2012; Yu et al., 2016; Zhang et al., 2015; Zhong et al., 2014, 2016). However, in a recent study, Lin et al. (2018a, 2018b) used zircon U—Pb ages, Hf isotopic data, and structural data to propose that the Wuyi–Yunkai orogenic belt was formed by oceanic subduction and the subsequent collision between the west Cathaysia Terrane and a yet-unidentified terrane that rifted away after the collision. Therefore, whether the formation of the early Paleozoic granites in South China was related to intracontinental orogeny or oceanic subduction remains uncertain.

We present detailed petrological, whole-rock major and trace element and Sr—Nd isotopic, and zircon U—Pb age and Hf—O isotopic data for the biotite, two-mica, and muscovite granites in the Baiyunshan and Maofengshan areas of Guangzhou, Guangdong Province, southeastern China. These data are used to constrain the time of formation of the granites and to infer their petrogenesis and tectonic setting.

2. Geological setting and sample descriptions

The South China Block (SCB) comprises the Yangtze Block to the northwest and the Cathaysia Block to the southeast, which collided during the Neoproterozoic along the Jiangshan–Shaoxing Fault (Fig. 1b; Zhao, 2015). The area between the Jiangshan–Shaoxing and Anhua–Luocheng faults is known as the eastern Yangtze Block (Fig. 1b). The basement of the eastern Yangtze Block is composed of Neoarchean and Paleoproterozoic tonalite–trondhjemite–granodiorite (TTG), felsic gneiss, and amphibolite (Wang et al., 2011b, and references therein). The basement of the Cathaysia Block is composed of Paleoproterozoic to early Neoproterozoic metamorphic rock (Chen and Jahn, 1998, and references therein). The Paleoproterozoic basement crops out mainly in southwestern Zhejiang Province (the Badu and Longquan groups) and in northwestern Fujian Province (the Mayuan and Mamianshan groups; Li et al., 1998). The Badu and Mayuan groups consist mainly of biotite plagioclase granulite, mica (quartz) schist, and minor amphibolite, whereas the Longquan and Mamianshan groups are composed chiefly of metamorphic volcanic and sedimentary rocks (Li et al., 1998). The Mesoproterozoic to Neoproterozoic basement crops out mostly in the center of Jiangxi Province (the Zhoutan Group) and consists of metasedimentary rock and metabasalt (Jiang and Zhu, 2017, and references therein).

After the Neoproterozoic Jinningian orogeny, which unified the Yangtze and Cathaysia blocks, the late Neoproterozoic Nanhua rift opened in Hunan, Jiangxi, western Guangdong, and eastern Guangxi provinces (Li et al., 2010; Wang and Li, 2003). The Nanhua basin was filled with siliciclastic rocks, volcaniclastic rocks, tuff, carbargilite, shale, and carbonates (Wang et al., 2011a). The lower Paleozoic strata consist of an interstratified carbonate–siliciclastic succession in the eastern Yangtze Block and a siliciclastic succession in the Cathaysia Block and are unconformably overlain by an upper Paleozoic succession (Wang et al., 2010).

Early Paleozoic magmatic rocks occur predominantly in the eastern Yangtze and Cathaysia blocks and are mostly S-type gneissic and massive granites that contain muscovite, garnet, or tourmaline (Shu et al., 2015; Wang et al., 2011b; Zhang et al., 2012). In addition, there are subordinate I-type (Guan et al., 2014; Huang et al., 2013; Xia et al., 2014; Xie et al., 2020; Yu et al., 2016) and A-type (Feng et al., 2014) granites, ultramafic to intermediate intrusive rocks (including diorite, pyroxene hornblendite, hornblende gabbro, and gabbro; Wang et al., 2013c; Zhong et al., 2014, 2016; Zhang et al., 2015; Jia et al., 2017; Zhao et al., 2019), volcanic rocks (basalts, andesites, and dacites; Yao et al., 2012), charnockites (Wang et al., 2013a), and metamorphic rocks (Li et al., 2010).

The Baiyunshan and Maofengshan areas lie in the south of the Wuyi–Yunkai orogen (Fig. 1c–d). The Baiyunshan area contains gneissic muscovite and massive two-mica granites, whereas the Maofengshan area contains only gneissic biotite granites. The biotite, two-mica, and muscovite granites in the Baiyunshan and Maofengshan areas were formed during the early Paleozoic (439–434 Ma; Yang et al., 2010). Carboniferous–Permian, Triassic, Jurassic, and Cretaceous sedimentary rocks are exposed around the Baiyunshan two-mica and muscovite granites (Fig. 1c), and the Maofengshan biotite granites are surrounded by a Mesoproterozoic gneissic complex (Fig. 1d).

The Baiyunshan muscovite granites are gray and pink, gneissic, fine grained (0.5–1.5 mm; Fig. 2a), and composed of quartz (40–45 vol%), muscovite (10–15 vol%), and feldspar (30–35 vol%) with minor zircon, apatite, monazite, and Fe—Ti oxides (Fig. 2d). They commonly have gneissic banding, with discontinuous quartz and muscovite foliation, and most of the feldspars have been replaced by sericites (Fig. 2d). The Baiyunshan two-mica granites are gray, massive, fine grained (0.5–1.0 mm; Fig. 2b), and composed of quartz (35–40 vol%), feldspar (30–35 vol%), muscovite (10–15 vol%), and biotite (3–5 vol%) with minor zircon, apatite, monazite, and Fe—Ti oxides (Fig. 2e–f). Most of the feldspars in the two-mica granites have also been replaced by sericites (Fig. 2e–f).

The Maofengshan biotite granites are dark gray, gneissic, fine to medium grained (0.5–2.5 mm; Fig. 2c), and composed of plagioclase (35–40 vol%), quartz (20–25 vol%), K-feldspar (10–15 vol%), and biotite (10–15 vol%), with minor zircon, apatite, monazite, and Fe—Ti oxides (Fig. 2g–h). They also show discontinuous subparallel biotite foliation (Fig. 2g).

3. Results

The analytical methods used during the study, including whole-rock major element, trace element, and Sr—Nd isotopic analyses, mineral composition analyses, zircon U—Pb age and Lu, Hf, and O isotopic analyses are presented in the Supplementary text 1.

3.1. Zircon U—Pb ages

Secondary ion mass spectrometry (SIMS) and laser ablation–inductively coupled plasma–mass spectrometry (LA–ICP–MS) zircon U—Pb ages of the biotite, two-mica, and muscovite granites are listed in Supplementary Table 1 and presented in Fig. 3. Most zircon grains are 100–200 μm in length and have aspect ratios of 2:1 to 4:1. Prismatic

Fig. 1. (a) Simplified regional map showing the tectonic framework of China (revised from Li et al., 2018). (b) Sketch map showing the distribution of early Paleozoic magmatic rocks in the South China Block (SCB). S-type granites are after Zhang et al. (2012) and Yu et al. (2019), I-type granites are after Huang et al. (2013), Yu et al. (2016), and Xie et al. (2020), A-type granites are after Feng et al. (2014), charnockites are after Wang et al. (2013a), ultramafic, mafic, and intermediate intrusive rocks are after Wang et al. (2013b), Zhong et al. (2014, 2016), Jia et al. (2017), and Zhao et al. (2019), and basalts, andesites, and dacites are after Yao et al. (2012). CNF: Changle–Nanao Fault, ZDF: Zhenghe–Dabu Fault, HGF: Heyuan–Guangfeng Fault, CLF: Chenzhou–Linwu Fault, JSF: Jiangshan–Shaoxing Fault, ALF: Anhua–Luocheng Fault. The solid blue line is the Yangtze River, the dotted black lines are provincial borders, and the solid black lines are national borders. Simplified geological maps of the (c) Baiyunshan and (d) Maofengshan areas [modified after Guangzhou Geological Maps at 1:250,000 scale (GDGBMR, 1988)], showing rock types and sample locations.

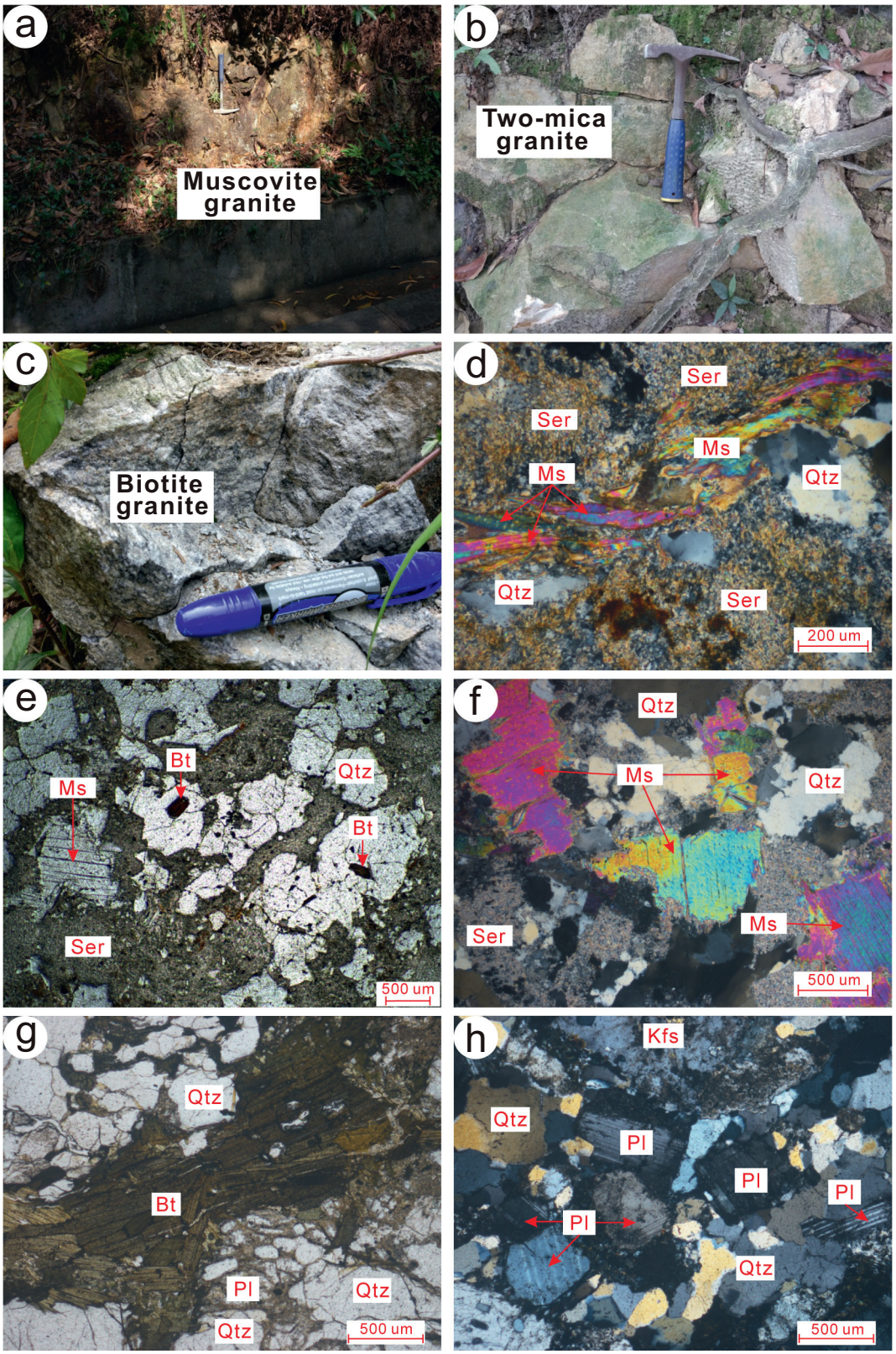

Fig. 2. Field photographs and photomicrographs of the Baiyunshan–Maofengshan granites. (a, d) Muscovite granites; (b, e, f) two-mica granites; (c, g, h) biotite granites. (e) and (g) were taken under plane-polarized light, and (d), (f), and (h) were taken under cross-polarized light. Bt: biotite, Kfs: K-feldspar, Ms: muscovite, Pl: plagioclase, Qtz: quartz, Ser: sericite.

zircon grains with clear oscillatory zonation (Fig. 3a–f, h) and high Th/U ratios (0.04–1.26; Supplementary Table 1) are interpreted to have a magmatic origin (Hoskin and Black, 2000), whereas those with a round or irregular shape (Fig. 3c–e, g) are suggested to be inherited zircons. Both types of zircon have narrow white metamorphic rims (Fig. 3a–f).

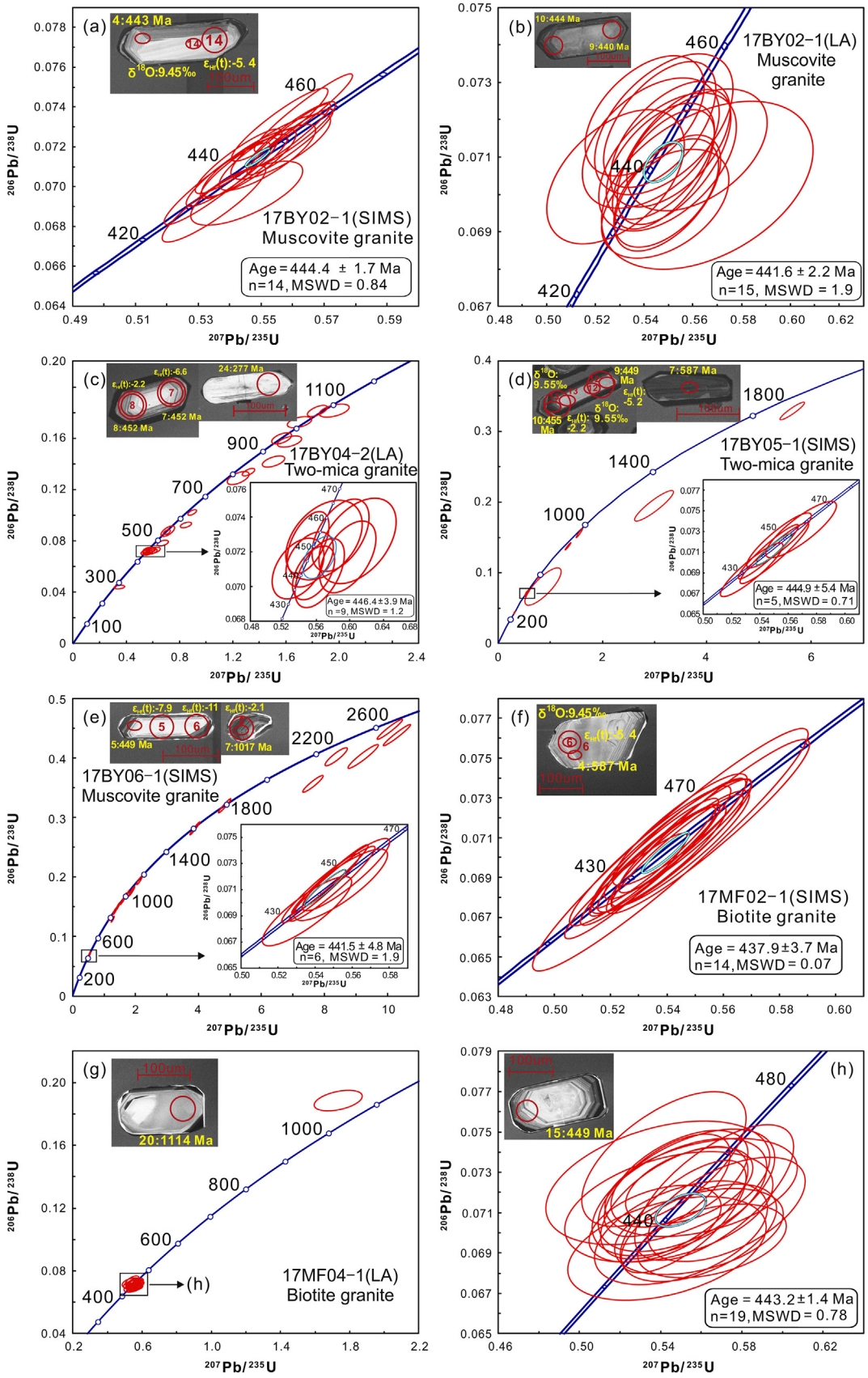

Fig. 3. SIMS and LA–ICP–MS zircon U-Pb concordia diagrams and cathodoluminescence (CL) images. (a, b) 17BY02-1 (Baiyunshan muscovite granite), (c) 17BY04-2 (Baiyunshan two-mica granite), (d) 17BY05-1 (Baiyunshan two-mica granite), (e) 17BY06-1 (Baiyunshan muscovite granite), (f) 17MF02-1 (Maofengshan biotite granite), (g, h) 17MF04-1 (Maofengshan biotite granite). Red circles on the CL images of zircon grains are SIMS or LA–ICP–MS analysis locations. Yellow numbers are ages and $\delta^{18}O$ and $\varepsilon_{Hf}(t)$ values.For interpretation of the references to colour in this figure legend, the reader is referred to the web version of this article.)

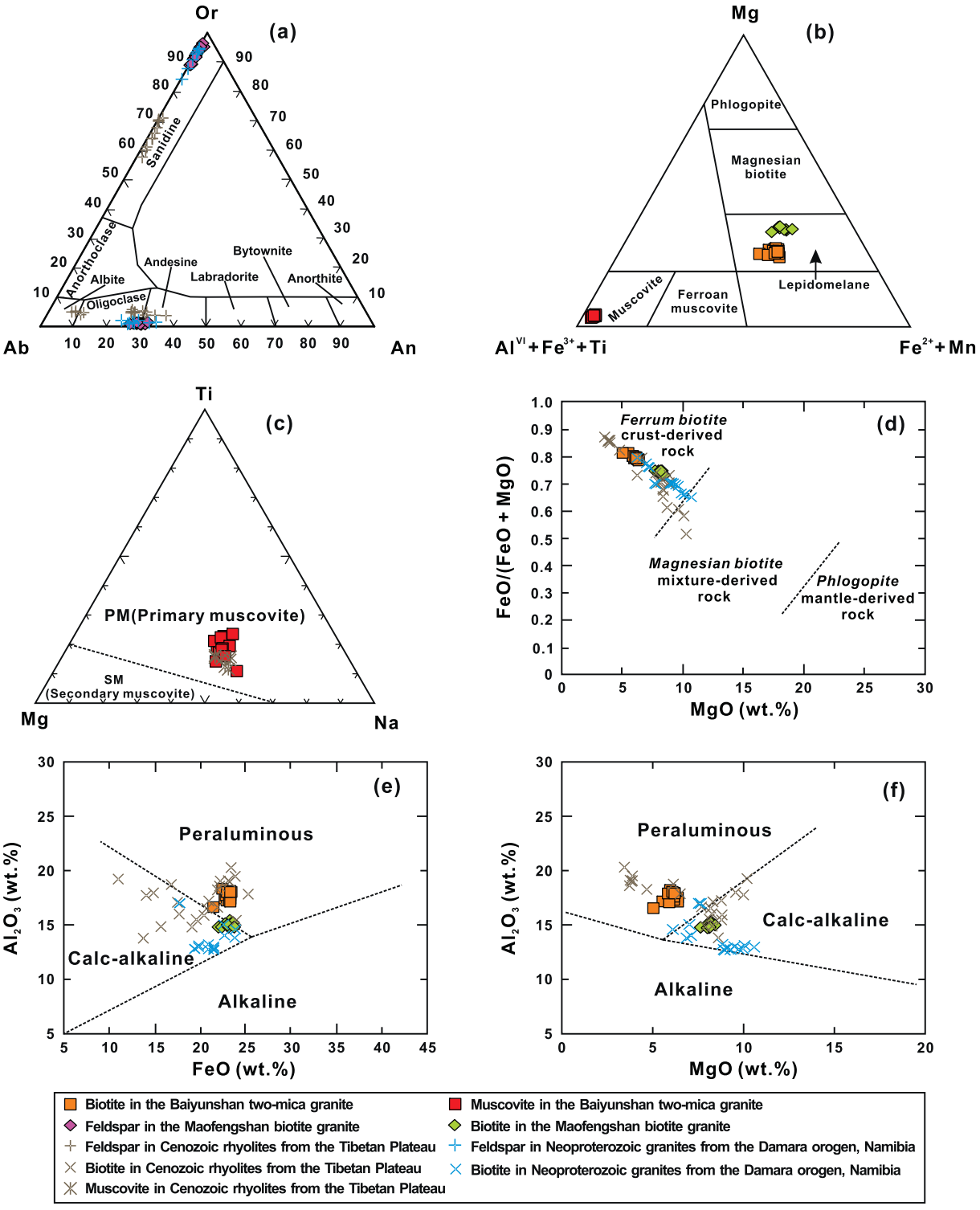

Fig. 4. Compositions of minerals in the Baiyunshan two-mica and Maofengshan biotite granites. (a) Feldspar Ab–Or–An diagram. Ab: albite, Or: K-feldspar, An: anorthite. (b) Mica ternary Mg–(Al^{VI} + Fe^{3+} + Ti)–(Fe^{2+} + Mn) diagram. (c) Muscovite ternary Mg–Ti–Na diagram (Miller et al., 1981); PM: primary muscovite, SM: secondary muscovite. (d) FeO/(FeO + MgO) versus MgO diagram for biotite (after Xia et al., 2014). (e) and (f) Al_2O_3 versus FeO and MgO diagrams for biotite classification (after Abdel Rahman, 1994). Data for feldspar, biotite, and muscovite in Cenozoic rhyolites from the Tibetan Plateau are from Wang et al. (2012). Data for feldspar and biotite in Neoproterozoic granites from the Damara orogen, Namibia, are from Jung et al. (1998).

SIMS U—Pb dating of zircons from the Baiyunshan muscovite granite sample 17BY02–1 yielded $^{206}Pb/^{238}U$ ages of 459–431 Ma, with a weighted mean age of 444.4 ± 1.7 Ma (2σ; MSWD = 0.84; n = 14; Fig. 3a; Supplementary Table 1), and muscovite granite sample 17BY06–1 yielded a weighted mean age of 441.5 ± 4.8 Ma (2σ; MSWD = 1.9; n = 6). The remaining 21 zircon grains yielded $^{206}Pb/^{238}U$ ages of 2752–783 Ma, which we interpret to be inherited ages (Fig. 3e; Supplementary Table 1). The two-mica granite sample 17BY05–1 yielded a weighted mean age of 444.9 ± 5.4 Ma (2σ; MSWD = 0.71; n = 5). Six zircon grains yielded $^{206}Pb/^{238}U$ ages of

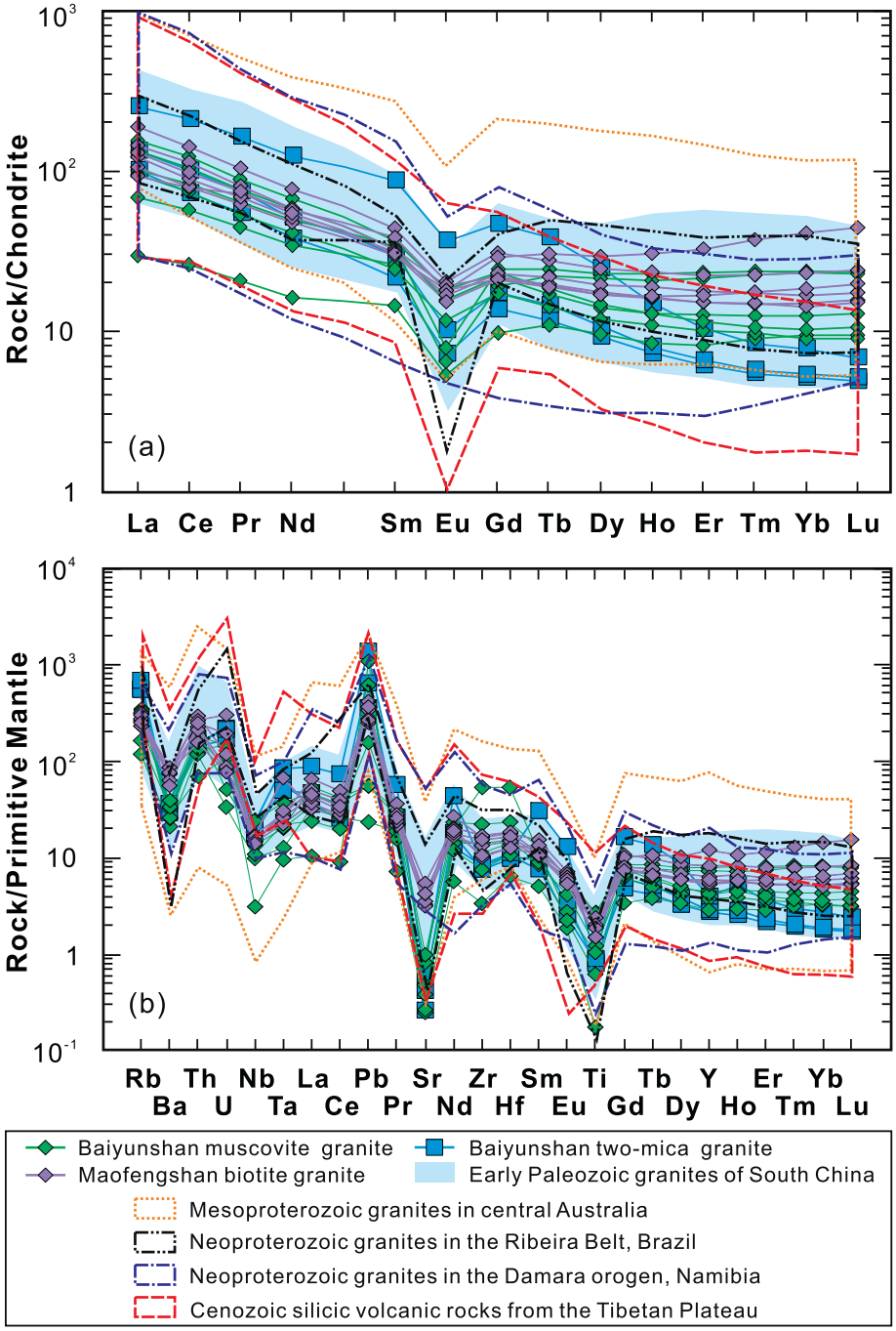

Fig. 5. (a) Chondrite-normalized REE and (b) primitive-mantle-normalized multi-element diagrams for the Baiyunshan–Maofengshan granites. Normalizing values are from Sun and McDonough (1989). Data for Mesoproterozoic granites in central Australia are from Smithies et al. (2011). Data for Neoproterozoic granites in the Ribeira Belt, Brazil, are from Passarelli et al. (2019). Data for Neoproterozoic granites in the Damara orogen, Namibia, are from Bergemann et al. (2014), Osterhus et al. (2014), and Stammeier et al. (2015). Data for early Paleozoic granites in the SCB are from Wang et al. (2011b) and Zhang et al. (2012). Data for Cenozoic silicic volcanic rocks from the Tibetan Plateau are from Wang et al. (2016).

1833–501 Ma, which we interpret to be inherited ages (Fig. 3d; Supplementary Table 1). The remaining zircon yielded a $^{206}Pb/^{238}U$ age of 278 Ma, which we suggest is a metamorphic age. The Maofengshan biotite granite sample 17MF02–1 yielded a weighted mean age of 437.9 ± 3.7 Ma (2σ; MSWD = 0.07; n = 14; Fig. 3f; Supplementary Table 1).

LA–ICP–MS U—Pb dating of zircons from the Baiyunshan muscovite granite sample 17BY02–1 yielded a weighted mean age of 441.6 ± 2.2 Ma (2σ; MSWD = 1.9; n = 15; Fig. 3b; Supplementary Table 1). The two-mica granite sample 17BY04–2 yielded a weighted mean age of 446.4 ± 3.9 Ma (2σ; MSWD = 1.2; n = 9). Fifteen zircon grains yielded $^{206}Pb/^{238}U$ ages of 2132–488 Ma, which we interpret to be inherited ages (Fig. 3c; Supplementary Table 1). The remaining zircon grain yielded a $^{206}Pb/^{238}U$ age of 277 Ma, inferred to be a metamorphic age (Fig. 3c; Supplementary Table 1). The Maofengshan biotite granite sample 17MF04–1 yielded a weighted mean age of 443.2 ± 1.4 Ma (2σ; MSWD = 0.78; n = 19; Fig. 3g–h; Supplementary Table 1). One zircon grain yielded a $^{206}Pb/^{238}U$ age of 1114 Ma, which we interpret to be an inherited age (Fig. 3g; Supplementary Table 1). In summary, the Baiyunshan–Maofengshan granites formed during the early Paleozoic (446–438 Ma).

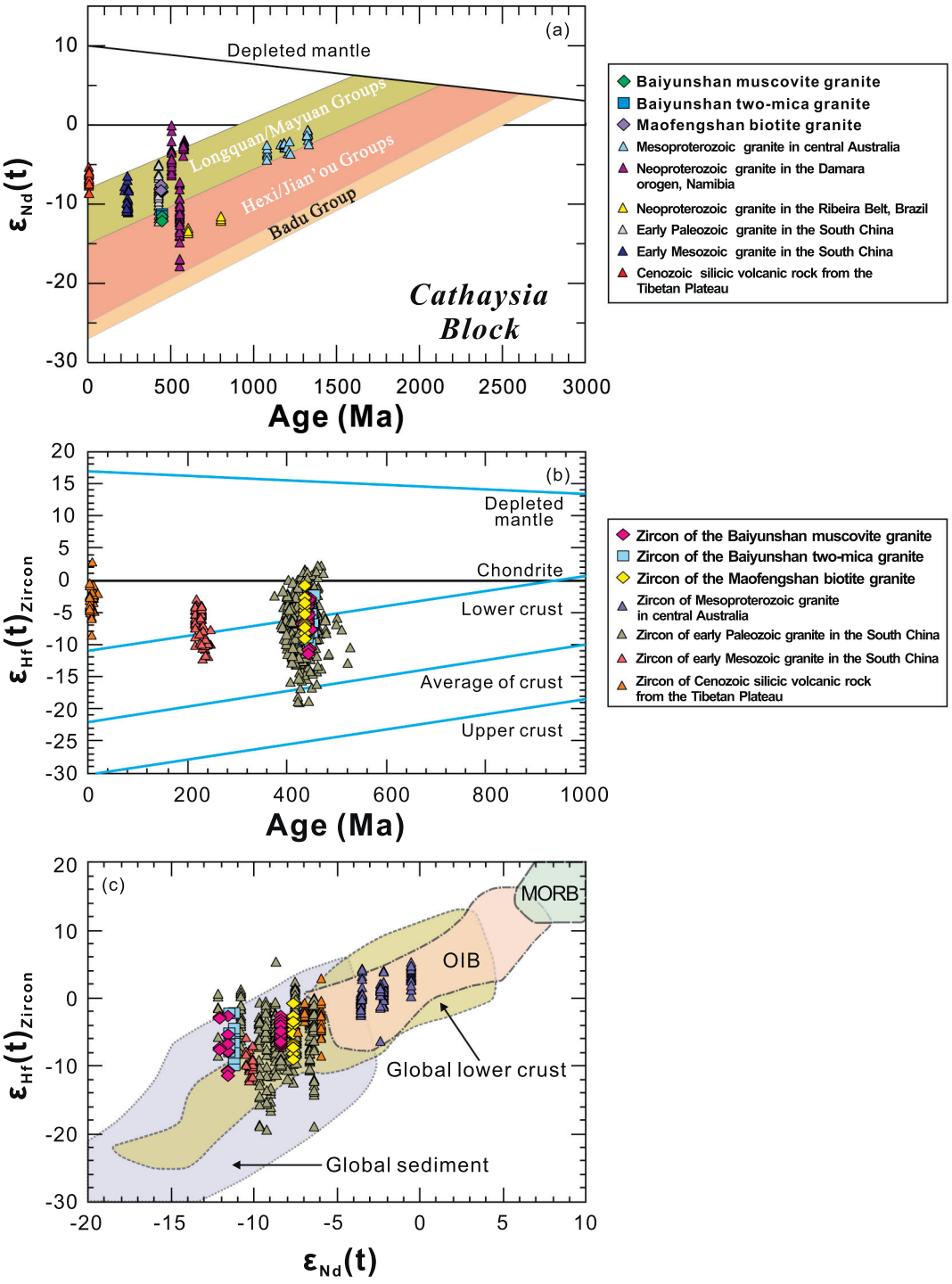

Fig. 6. (a) Nd isotopic evolution of the Cathaysia Block (modified from Chen and Jahn, 1998). (b) Hf isotopic evolution of magmatic zircons from the Baiyunshan–Maofengshan granites. Depleted mantle has present-day $^{176}Lu/^{177}Hf$ and $^{176}Hf/^{177}Hf$ ratios of 0.0384 and 0.28325, respectively (Griffin et al., 2000), chondrite has present-day $^{176}Lu/^{177}Hf$ and $^{176}Hf/^{177}Hf$ ratios of 0.0332 and 0.28277, respectively (Wu et al., 2007, and references therein), continental upper crust has a present-day $^{176}Lu/^{177}Hf$ ratio of 0.0093, average crust has a present-day $^{176}Lu/^{177}Hf$ ratio of 0.015, and lower crust has a present-day $^{176}Lu/^{177}Hf$ ratio of 0.022 (Wu et al., 2007, and references therein). (c) Zircon $\varepsilon_{Hf}(t)$ values versus whole-rock $\varepsilon_{Nd}(t)$ values for the Baiyunshan–Maofengshan granites. OIB: ocean island basalt, MORB: mid-ocean ridge basalt. The global lower crust and sediment fields are from Dobosi et al. (2003). Data for early Paleozoic granites in the SCB are from Wang et al. (2011b) and Zhang et al. (2012), respectively. Data for early Mesozoic granites in the SCB are from Wang et al. (2007); Gao et al. (2014); Shu et al. (2015). Data for global intracontinental igneous rocks are the same as in Fig. 5.

3.2. Mineral compositions

Mineral composition data for the granites are listed in Supplementary Table 2. In the Maofengshan biotite granite, the plagioclase crystals are andesine and oligoclase ($An_{27-31}Ab_{67-72}Or_{1-2}$; Fig. 4a; Supplementary Table 2), and the K-feldspar crystals are sanidine ($An_{0-1}Ab_{3-10}Or_{90-97}$; Fig. 4a; Supplementary Table 2). Feldspar compositions of the Maofengshan biotite granite are similar to feldspars in Cenozoic rhyolites from the Tibetan Plateau and Neoproterozoic granites of the Damara orogen, Namibia (Fig. 4a). Plagioclases in the Maofengshan biotites have SiO_2 (59.3–62.0 wt% and 58.9–66.2 wt%, respectively) and CaO (5.80–6.83 wt% and 1.48–7.48 wt%, respectively)

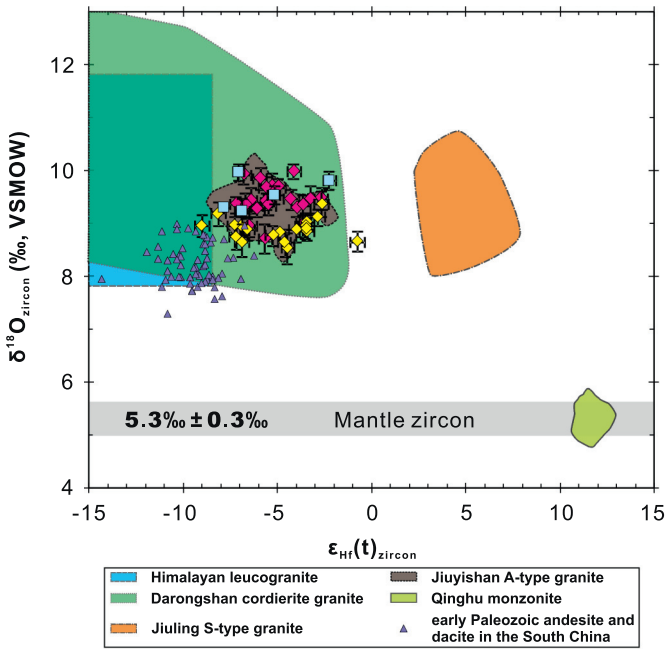

Fig. 7. O versus Hf isotopic compositions of the zircon in the Baiyunshan–Maofengshan granites. Data for the Qinghu monzonite, Jiuyishan A-type granite, Darongshan cordierite granite, Jiuling S-type granite, and Himalayan leucogranite are from Liu et al. (2020), and references therein. Data for early Paleozoic andesites and dacites in the SCB are from Yao et al. (2012). The legend is the same as in Fig. 6.

contents similar to those of Cenozoic rhyolites from the Tibetan Plateau and Neoproterozoic granites of the Damara orogen, Namibia (Supplementary Fig. 1e; Supplementary Table 2). The biotite crystals in both the Baiyunshan two-mica and Maofengshan biotite granites are lepidomelane (Fig. 4b), but the biotite in the latter has higher MgO contents (6.57–8.47 wt%) than those in the former (5.07–6.42 wt%; Supplementary Table 2). Biotites in the Baiyunshan–Maofengshan granites have similar Al_2O_3, FeO (14.8–18.3 and 21.6–24.0 wt%, respectively; Supplementary Table 2), and MgO contents as those in Cenozoic rhyolites from the Tibetan Plateau (13.9–20.4, 10.8–25.2, and 3.4–10.2 wt%, respectively; Fig. 4d–f). However, biotites in the Baiyunshan–Maofengshan granites have higher Al_2O_3 and FeO and lower MgO contents than those in Neoproterozoic granites of the Damara orogen, Namibia (12.7–17.0, 17.7–23.8, and 6.1–10.6 wt%, respectively; Fig. 4d–f). Biotites in the Baiyunshan–Maofengshan granites overall have lower TiO_2 (2.05–2.79 wt% and 1.89–4.43 wt%, respectively) contents than those in Cenozoic rhyolites from the Tibetan Plateau and Neoproterozoic granites of the Damara orogen, Namibia (Supplementary Fig. 1f; Supplementary Table 2). The muscovite crystals in the Baiyunshan two-mica granite are primary, with MgO contents of 0.61–0.85 wt%, TiO_2 contents of 0.47–1.1 wt%, and Na_2O contents of 0.58–0.91 wt% (Fig. 4c; Supplementary Table 2). Muscovite compositions of the Baiyunshan two-mica granites are also similar to those in Cenozoic rhyolites from the Tibetan Plateau (Fig. 4c).

3.3. Whole-rock major and trace element compositions

Whole-rock major and trace element data for the biotite, two-mica, and muscovite granites are listed in Supplementary Table 3. The Baiyunshan two-mica and muscovite granites have high SiO_2 (72.6–80.4 wt%) and K_2O (3.19–5.32 wt%) and low MgO (0.46–0.77 wt%) contents (Supplementary Table 3). The two-mica granites have lower SiO_2 (72.6–74.9 wt%) and higher MgO (0.69–0.77 wt%) and K_2O (4.85–5.32 wt%) contents than the muscovite granites (SiO_2 = 76.7–80.4 wt%, MgO = 0.46–0.61 wt%, K_2O = 3.19–4.31 wt%; Supplementary Table 3). The Maofengshan biotite granites have high SiO_2 (69.0–73.5 wt%), K_2O (3.40–4.62 wt%), and Na_2O (2.02–3.58 wt%) contents, with $K_2O > Na_2O$ (Supplementary Table 3). The Maofengshan granites have lower SiO_2 and higher MgO contents (0.61–1.17 wt%) than those of the Baiyunshan granites (Supplementary Table 3). The Maofengshan granites have SiO_2, Al_2O_3 (13.0–15.0 wt%), TiO_2 (0.33–0.53 wt%), $Fe_2O_3^T$ (2.11–3.75 wt%), and MgO contents similar to those of Neoproterozoic granites in the Ribeira Belt (Brazil) and early Mesozoic granites in the SCB (68.3–76.5, 12.9–15.0, 0.03–0.83, 0.70–3.80, and 0.04–2.30 wt%, respectively; Supplementary Fig. 1a–d; Supplementary Table 3). However, the Maofengshan granites exhibit smaller variation ranges of SiO_2, Al_2O_3, TiO_2, $Fe_2O_3^T$, and MgO contents than Mesoproterozoic granites in central Australia, Neoproterozoic granites in the Damara orogen (Namibia), early Paleozoic granites in the SCB, and Cenozoic silicic volcanic rocks from the Tibetan Plateau (60.2–78.1, 10.2–17.6, 0.02–2.06, 0.08–16.3, and 0.02–5.11 wt%, respectively; Supplementary Fig. 1a–d).

The Maofengshan biotite and Baiyunshan muscovite granites exhibit slight to moderate enrichment in light rare-earth elements (LREEs) [$(La/Yb)_{CN}$ = 2.27–15.1, where "CN" indicates chondrite-normalized values] and slight to pronounced negative Eu anomalies ($Eu/Eu^* = Eu_{CN}/(Sm_{CN} \times Gd_{CN})^{1/2}$ = 0.27–0.72) in a chondrite-normalized REE variation diagram (Fig. 5a). The Baiyunshan two-mica granites are more clearly enriched in LREEs [$(La/Yb)_{CN}$ = 19.6–32.1] compared with the biotite or muscovite granites and have moderate negative Eu anomalies (Eu/Eu^* = 0.42–0.58; Fig. 5a). In a primitive-mantle-normalized diagram, both of these granites are enriched in Rb, Th, U, and Pb and depleted in Ba, Sr, Nb, and Ti (Fig. 5b). The Baiyunshan–Maofengshan granites have similar REE and trace element compositions as Neoproterozoic granites in the Ribeira Belt (Brazil) and Damara orogen (Namibia) (Fig. 5a–b). However, the Baiyunshan–Maofengshan granites have lower ΣREE contents (44.2–302.3 and 43.7–1995 ppm, respectively; Supplementary Table 3; Smithies et al., 2011) and trace element contents than Mesoproterozoic high-temperature granites in central Australia (Fig. 5a–b). In addition, the Baiyunshan–Maofengshan granites also exhibit less fractionated REE patterns than Cenozoic, thickened crust-derived, silicic volcanic rocks from the Tibetan Plateau (Fig. 5a–b; $(La/Yb)_{CN}$ = 6.75–94.8; Wang et al., 2016).

3.4. Sr–Nd–Hf–O isotopic compositions

Whole-rock Sr—Nd and zircon Hf—O isotopic data for the granites are listed in Supplementary Tables 3 and 4. On the basis of the zircon U—Pb ages, initial Nd isotopic ratios were calculated at 444 Ma for the Baiyunshan granites and at 438 Ma for the Maofengshan granites. Initial Hf isotopic ratios were calculated using the corresponding zircon single-crystal ages. The granites have variable $\varepsilon_{Nd}(t)$ values (−12.1 to −7.6) (Fig. 6a, c; Supplementary Table 3). As the granites have exceptionally high $^{87}Rb/^{86}Sr$ ratios (6.29 to 124; Supplementary Table 3), we did not calculate their initial $^{87}Sr/^{86}Sr$ ratios. Magmatic zircon grains in the granites have variable initial $^{176}Hf/^{177}Hf$ ratios (0.282172–0.282477) and $\varepsilon_{Hf}(t)$ values (−11.4 to −0.8; Figs. 6b–c, 7; Supplementary Table 4), and the inherited zircon grains have a wider range of initial $^{176}Hf/^{177}Hf$ ratios (0.280825–0.282595) and $\varepsilon_{Hf}(t)$ values (−27.0 to +10.7; Supplementary Table 4). The magmatic zircon has high and relatively homogeneous $\delta^{18}O$ values (8.5‰–10.0‰; Fig. 7; Supplementary Table 4) with an average of 9.23‰ ± 0.39‰ (SD).

4. Discussion

4.1. Effects of metamorphism and alteration

The granites have undergone low-grade metamorphism, as shown by the common narrow white rims on zircon crystals (Fig. 3a–f), and have been weathered at the surface (Fig. 2a–c), which means that it is important to evaluate the effects of metamorphism and alteration on

their compositions before using geochemistry to investigate their petrogenesis. The transition elements (e.g., Cr and Ni), REEs, high-field-strength elements (HFSEs; e.g., Nb, Ta, Zr, and Hf), and Th remain stable during low-grade metamorphism and alteration (Wang et al., 2006). Large-ion lithophile elements (LILEs; e.g., Rb, Ba, and Sr) are usually mobile during low-temperature alteration (Hawkesworth et al., 1997). The SiO_2, TiO_2, Al_2O_3, $Fe_2O_3^T$, and MgO contents of the Maofengshan biotite granites show no obvious variation with increasing loss-on-ignition (LOI; Supplementary Fig. 2a–d, f), indicating that they represent original compositions. In contrast, the CaO, Na_2O, and K_2O contents of the Maofengshan biotite granites and the SiO_2, TiO_2, Al_2O_3, $Fe_2O_3^T$, K_2O, and MgO contents of the Baiyunshan two-mica and muscovite granites are correlated with LOI (Supplementary Fig. 2a–h). In particular, the Ca and Na in the Baiyunshan two-mica and muscovite granites were nearly completely leached during low-grade metamorphism and alteration (Supplementary Fig. 2g, h). The two Baiyunshan muscovite granites that have abnormal SiO_2 and K_2O contents (89.0–89.1 wt% and 1.50–1.96 wt%, respectively; Supplementary Table 3) possibly underwent the most intense supergene weathering of all the studied samples. Here, we focus on immobile elements, including SiO_2, TiO_2, Al_2O_3, $Fe_2O_3^T$, MgO (only in the Maofengshan biotite granites), HFSEs (Nb, Ta, Zr, and Hf), REEs, Th, and transition elements (Cr and Ni) in our discussion of the petrogenesis of the granites.

The Nd isotopic compositions of magmatic rocks are little affected by low-grade metamorphism and alteration, whereas Sr isotopic compositions are susceptible to change (Wang et al., 2006). Given that the $\varepsilon_{Nd}(t)$ values of the granites show almost no correlation with LOI (Supplementary Fig. 2i), we suggest that the Nd isotopic compositions of these granites represent primary compositions. In addition, zircon is a stable accessory mineral that preserves the O and Hf isotopic and trace element compositions of its host magma during crystallization (Li et al., 2009). Therefore, we used whole-rock Nd isotopic data and zircon Hf—O isotopic and Ti data to reveal the petrogenesis of the granites.

4.2. Petrogenesis

4.2.1. Crustal contamination and magma mixing

The whole-rock $\varepsilon_{Nd}(t)$ values, zircon Hf—O isotopic compositions, petrographic characteristics, and mineral compositions of the studied granites cannot be reproduced by modeling the effects of crustal contamination on mantle-derived magma, or by mixing mantle- and crust-derived magmas. In general, old crustal rocks and their melts have enriched Nd isotopic compositions (Ma et al., 2017, and references therein), whereas juvenile crustal rocks and their melts have depleted Nd isotopic compositions (Jiang et al., 2018, and references therein); therefore, crustal contamination or magma mixing during magma ascent would lead to variable $\varepsilon_{Nd}(t)$ values. The $\varepsilon_{Nd}(t)$ values of the granites show no correlation with their SiO_2 contents (Supplementary Fig. 3a). In addition, there is a lack of correlation between $(^{147}Sm/^{144}Nd)_s$ and initial $^{143}Nd/^{144}Nd$ ratios for the granites (Supplementary Fig. 3b). Although the granites have a wide range of $\varepsilon_{Nd}(t)$ values (−12.1 to −7.6; Fig. 6a, c; Supplementary Table 3), this may have resulted from heterogeneity of their source rock (discussed below) rather than crustal contamination or magma mixing. In addition, the granites have a limited range of zircon Hf—O isotopic compositions ($\varepsilon_{Hf}(t) = -11.4$ to −0.8; $\delta^{18}O = 8.5‰–10.0‰$; Fig. 7; Supplementary Table 4) and smaller variations in $\varepsilon_{Hf}(t)$ values (−16.0 to +9.0) compared with the early Paleozoic I-type granites in the eastern Yangtze and Cathaysia blocks that are thought to have been formed by mixing between mantle-derived mafic and crust-derived felsic magmas (Huang et al., 2013; Xia et al., 2014; Yu et al., 2016; Zhang et al., 2015). In an $\varepsilon_{Hf}(t)$ versus $\delta^{18}O$ diagram, the granites do not fall on a mixing trend between mafic and felsic magmas (Fig. 7). Moreover, the early Paleozoic granites in the eastern Yangtze and Cathaysia blocks that were formed by magma mixing generally contain mafic microgranular enclaves (Guan et al., 2014; Xia et al., 2014; Xu and Xu, 2015; Yu et al., 2016), which are absent in the Baiyunshan–Maofengshan granites (Fig. 2a–c). The Baiyunshan–Maofengshan granites also have more enriched Nd—Hf isotopic compositions and smaller variations in Nd isotopic compositions when compared with Mesoproterozoic granites in central Australia ($\varepsilon_{Nd}(t) = -4.4$ to −0.6; $\varepsilon_{Hf}(t) = -6.3$ to +5.3) and Neoproterozoic granites in the Damara orogen, Namibia ($\varepsilon_{Nd}(t) = -17.8$ to −0.03), which were formed by crust–mantle interaction (Jung et al., 1998; Smithies et al., 2011; Fig. 6a, c). Furthermore, biotites in the studied granites are Fe-rich biotites that crystallized from pure crust-derived magmas (Xia et al., 2014; Fig. 4d).

4.2.2. Fractional crystallization

The granites may have undergone biotite, plagioclase, K-feldspar, Fe–Ti-oxide, and REE-enriched mineral fractionation. In Harker diagrams, the Al_2O_3, TiO_2, $Fe_2O_3^T$, and MgO contents of the Maofengshan biotite granites gradually decrease with increasing SiO_2 content (Supplementary Fig. 1a–d). This trend indicates the separation of biotite and Fe—Ti oxides, which are enriched in these elements. Given that plagioclase is enriched in CaO, the negative relationship between the CaO and SiO_2 contents of the plagioclase in the Maofengshan biotite granites suggests fractionation of plagioclase (Supplementary Fig. 1e). Similarly, the negative correlation between the TiO_2 and SiO_2 contents of the biotite crystals in the Baiyunshan two-mica and Maofengshan biotite granites suggests biotite fractionation (Supplementary Fig. 1f). In addition, the wide range of REE contents of the granites (ΣREE = 44.2–302.5 ppm; Fig. 5a; Supplementary Table 3) suggests fractionation of REE-enriched minerals, such as monazite (Yang et al., 2019, and references therein). The variable Eu/Eu^* (0.27–0.72) values and negative Ba and Sr anomalies of the granites (Fig. 5b; Supplementary Table 3) also suggest fractionation of plagioclase and K-feldspar.

4.2.3. Partial melting

The whole-rock major element, trace element, and Nd isotopic compositions and zircon Hf—O isotopic compositions of the granites suggest that the primary magma was not derived from the mantle or juvenile crust. The granites have higher SiO_2 (69.0–80.4 wt%) and lower MgO (0.46–1.17 wt%), Cr (1.74–54.6 ppm), and Ni (0.51–6.17 ppm) contents than those of early Paleozoic ultramafic to intermediate rocks in the Cathaysia Block (SiO_2 = 44.8–65.0 wt%, MgO = 1.87–24.6 wt%, Cr = 27.0–2328 ppm, Ni = 9.00–805 ppm; Supplementary Table 3; Yao et al., 2012; Wang et al., 2013c; Zhong et al., 2014, 2016; Zhang et al., 2015). The removal of a significant volume of mafic minerals would be required to produce the major and trace element compositions of the granites; however, they do not contain the mafic minerals that commonly crystallize in mantle-derived mafic magmas such as pyroxene and olivine (Fig. 2d–h). In addition, the granites have more enriched whole-rock Nd isotopic compositions ($\varepsilon_{Nd}(t) = -12.1$ to −7.6) relative to early Paleozoic sub-continental lithospheric mantle-derived rocks in the Cathaysia Block ($\varepsilon_{Nd}(t) = -9.8$ to −0.6; Fig. 6a, c; Supplementary Table 3; Yao et al., 2012; Wang et al., 2013c; Zhong et al., 2014, 2016; Zhang et al., 2015). Moreover, the granites also have slightly higher zircon $\delta^{18}O$ values (8.5‰–10.0‰) than the high-Mg andesites that are thought to be the product of assimilation and fractional crystallization (AFC) of early Paleozoic basalts in the Cathaysia Block (7.3‰–9.0‰; Yao et al., 2012; Fig. 7). Furthermore, the granites also have higher zircon $\delta^{18}O$ values than the Paleocene, juvenile crust-derived, Zhengga biotite and two-mica granites ($\delta^{18}O = 5.5‰–7.3‰$; Ma et al., 2017) in southern Tibet. Therefore, the granites were not formed by fractional crystallization of mantle- or juvenile crust-derived magmas.

We suggest that the Baiyunshan granites were derived by partial melting of metasedimentary rocks, while the Maofengshan granites were derived by partial melting of a hybridized crustal source dominated by metasedimentary rocks with subordinate amphibolites. The compositions of most biotites in the studied granites plot in the field for biotite from peraluminous granites (i.e., S-type granites) (Fig. 4e).

In addition, the granites have similar Th contents (5.93–25.2 ppm), Th/La ratios (0.23–1.02), and Nb/Ta ratios (4.25–14.7) to those of the metasediment-derived Himalayan leucogranites (Th: 1.35–21.5 ppm; Th/La: 0.23–1.88; Nb/Ta: 3.74–16.0; Guo and Wilson, 2012; Supplementary Table 3). The granites also have similar trace element and isotopic compositions as Neoproterozoic granites in the Ribeira Belt, Brazil ($\varepsilon_{Nd}(t) = -13.7$ to -11.5), early Paleozoic ($\varepsilon_{Nd}(t) = -11.4$ to -5.0; $\varepsilon_{Hf}(t) = -15.2$ to $+2.4$) and early Mesozoic ($\varepsilon_{Nd}(t) = -11.0$ to -6.4; $\varepsilon_{Hf}(t) = -12.2$ to -2.8) granites in the SCB, and Cenozoic silicic volcanic rocks from the Tibetan Plateau ($\varepsilon_{Nd}(t) = -8.6$ to -5.3; $\varepsilon_{Hf}(t) = -8.5$ to $+2.9$), which were derived from a crustal metasediment-dominated source (Fig. 6a–c). Moreover, zircons that crystallized in the Baiyunshan–Maofengshan granites have high $\delta^{18}O$ values (8.5‰–10.0‰; Fig. 7; Supplementary Table 4) that are similar to those of zircons that crystallized from metasediment-derived Himalayan leucogranites, Neoproterozoic Jiuling S-type granites, Triassic Darongshan cordierite-bearing granites, and Jurassic Jiuyishan A-type granites in the SCB ($\delta^{18}O = 8.2$‰ to 12.9‰; Fig. 7).

Experimental data indicate that sediment-derived melts have $SiO_2 \geq 70$ wt% (Patiño Douce, 1999). However, one Maofengshan biotite granite sample has $SiO_2 < 70$ wt% (17MF02–2; 69.0 wt%; Supplementary Table 3). In addition, biotites in the Maofengshan biotite granites plot in the fields for peraluminous granites (S-type granites) and calc-alkaline granites (I-type granites; Fig. 4e–f). Therefore, in addition to metasedimentary rocks, metaigneous rocks were possibly involved in the source of the Maofengshan biotite granites. The metamorphic basement of the eastern SCB consists of paragneiss, migmatite, schist, and amphibolite (Zhang et al., 2012, and references therein), and we suggest that amphibolites were part of the metasedimentary rock-dominated source of the Maofengshan biotite granites.

Primary muscovite can be used to constrain the pressure of its host magma (Huang et al., 2015, and references therein). The low $FeO^T + MgO$ contents of the high-Ti (>0.4 wt%) primary muscovite in the Baiyunshan two-mica granite are consistent with low proportions of celadonite (Supplementary Table 2), suggesting that they crystallized at high temperatures (Miller et al., 1981). The Si-in-muscovite barometer (Anderson, 1996) gives a pressure of 6.2 ± 0.3 kbar (1σ; ~20 km) assuming a magma temperature of 700 °C and a pressure gradient of 3.3 km/kbar. We estimated the crystallization temperature of the Baiyunshan two-mica granite using the Ti-in-zircon (T_{Ti-Zr}) thermometer of Ferry and Watson (2007). Because quartz occurs as a major phase in the Baiyunshan two-mica granite, we can assume that $\alpha_{SiO2} = 1$. Although rutile is absent in the Baiyunshan two-mica granite, most silicic magmas have α_{TiO2} values of about 0.6–0.9 (Ferry and Watson, 2007); therefore, our Ti-in-zircon temperature estimates assume that $\alpha_{TiO2} = 0.7$ in the Baiyunshan two-mica granite. The T_{Ti-Zr} estimates for the Baiyunshan two-mica granite are 600–773 °C (mean = 708 °C; Supplementary Table 1). An experimental study of leucogranites suggested that primary muscovite can crystallize at ~700 °C (Scaillet et al., 1995), meaning that it is reasonable to estimate the formation pressure of muscovite using a temperature of 700 °C. The Baiyunshan muscovite and Maofengshan biotite granites (Fig. 3a, b, e–h) were coeval with the Baiyunshan two-mica granites (Fig. 3c, d), have similar Nd–Hf–O isotopic compositions (Figs. 6, 7; Supplementary Tables 3–4), and were derived from a metasediment-dominated crustal source. Therefore, the melting that produced the Baiyunshan muscovite and Maofengshan biotite granites might have also occurred in the middle to upper crust.

Experimental studies have shown that mica might start to break down at above 700 °C and 5 kbar (Patiño Douce and Harris, 1998). The Maofengshan biotite granite, Baiyunshan two-mica granite, and Baiyunshan muscovite granite have average Ti-in-zircon temperatures of 687, 708, and 746 °C (Supplementary Table 1), respectively, which represent the minimum temperatures of the magma source. Therefore, we suggest that the granites were generated mainly by partial melting of metasedimentary rocks due to mica dehydration.

4.3. Geodynamic processes and implications for intracontinental orogeny

Whether the widely distributed early Paleozoic granites in the SCB were formed in an intracontinental orogenic or an oceanic subduction setting remains unresolved (Wang et al., 2011b, and references therein; Shu et al., 2015, Shu et al., 2018; Lin et al., 2018a, 2018b). We suggest that the Baiyunshan–Maofengshan granites were more likely formed in an intracontinental setting rather than a subduction–collision setting. Early Paleozoic, arc-like, mafic intrusive and volcanic rocks in the SCB originated from Neoproterozoic metasomatized lithospheric mantle rather than Paleozoic metasomatized lithospheric mantle (Wang et al., 2013c; Zhang et al., 2015; Zhong et al., 2014, 2016). In addition, the absence of ophiolites, high-pressure–low-temperature metamorphic rocks, and turbidites in the SCB is inconsistent with a subduction setting (Shu et al., 2015; Shu et al., 2018; Wang et al., 2011b). Moreover, the coherent biostratigraphy and paleoecology (Chen et al., 2010), continuous sedimentary facies, and similar detrital zircon ages (Wang et al., 2010) across the Cathaysia and Yangtze blocks during the early Paleozoic suggest there was no ocean between these two blocks at that time.

The Baiyunshan–Maofengshan granites, along with the early Paleozoic S-type granites in the SCB, are distributed over an area of 1200 km × 600 km (Shu et al., 2015, Shu et al., 2018; Fig. 1b), in contrast to the linear distribution of magmatic rocks typically found in subduction–collision orogenic belts (e.g., Morris et al., 2019). In addition, the Baiyunshan–Maofengshan granites have different temporal and spatial distribution patterns as compared with late Mesozoic granites and volcanic rocks in the SCB. With roll-back of the Paleo-Pacific Plate, late Mesozoic magmatism propagated from the inland to coastal region (Li et al., 2013; Li and Li, 2007; Zhou and Li, 2000). Compared with the late Mesozoic granites and volcanic rocks, the early Paleozoic S-type granites in the SCB generally do not show younging trends from east (coastal provinces) to west (Xuefeng) or from south (Yunkai) to north (Jiangnan) (Fig. 1b; Wang et al., 2013b). Moreover, on tectonic discrimination diagram, the Baiyunshan–Maofengshan granites plot either in the syn–collisional or post–collisional fields rather than volcanic arc field (Supplementary Fig. 4). Therefore, the Baiyunshan–Maofengshan granites were likely formed in an intracontinental setting rather than a subduction–collision setting.

Several different geodynamic models have been proposed for the formation and evolution of the early Paleozoic intracontinental orogen in the SCB: intracontinental subduction of the Cathaysia Block beneath the Yangtze Block (Faure et al., 2009); northwestward subduction of the inferred East China Sea Block and southeastward underthrusting of the Yangtze Block beneath the Cathaysia Block (Shu et al., 2015, and references therein); northwestward overthrusting of the Cathaysia Block onto the foreland basin at the southeastern margin of the Yangtze Block (Li et al., 2010). Asthenospheric upwelling was triggered by stress originating from the plate boundary during the break-up of Gondwana (Xu and Xu, 2015). Further crustal thickening was linked to the far-field response to the amalgamation of the Australian–Indian Plate with the Cathaysia Block (Wang et al., 2011b; Zhang et al., 2012) and subsequent post-orogenic lithospheric delamination (Wang et al., 2013c; Yao et al., 2012; Yu et al., 2016; Zhang et al., 2015). Syn-convergent extension and asthenospheric upwelling were caused by reactivation of a series of NW–SE-trending strike-slip faults and a NE–SW-trending rift zone during the intracontinental orogeny (Xie et al., 2020).

There were no asthenospheric or lithospheric mantle-derived magmas involved in the crustal source of the Baiyunshan–Maofengshan granites. In addition, early Paleozoic intermediate–mafic igneous rocks and mafic microgranular enclave-bearing granites have not been discovered in the Guangzhou region. Therefore, we prefer the intraplate subduction or overthrusting models to explain the origins of the Baiyunshan–Maofengshan granites. The SCB underwent

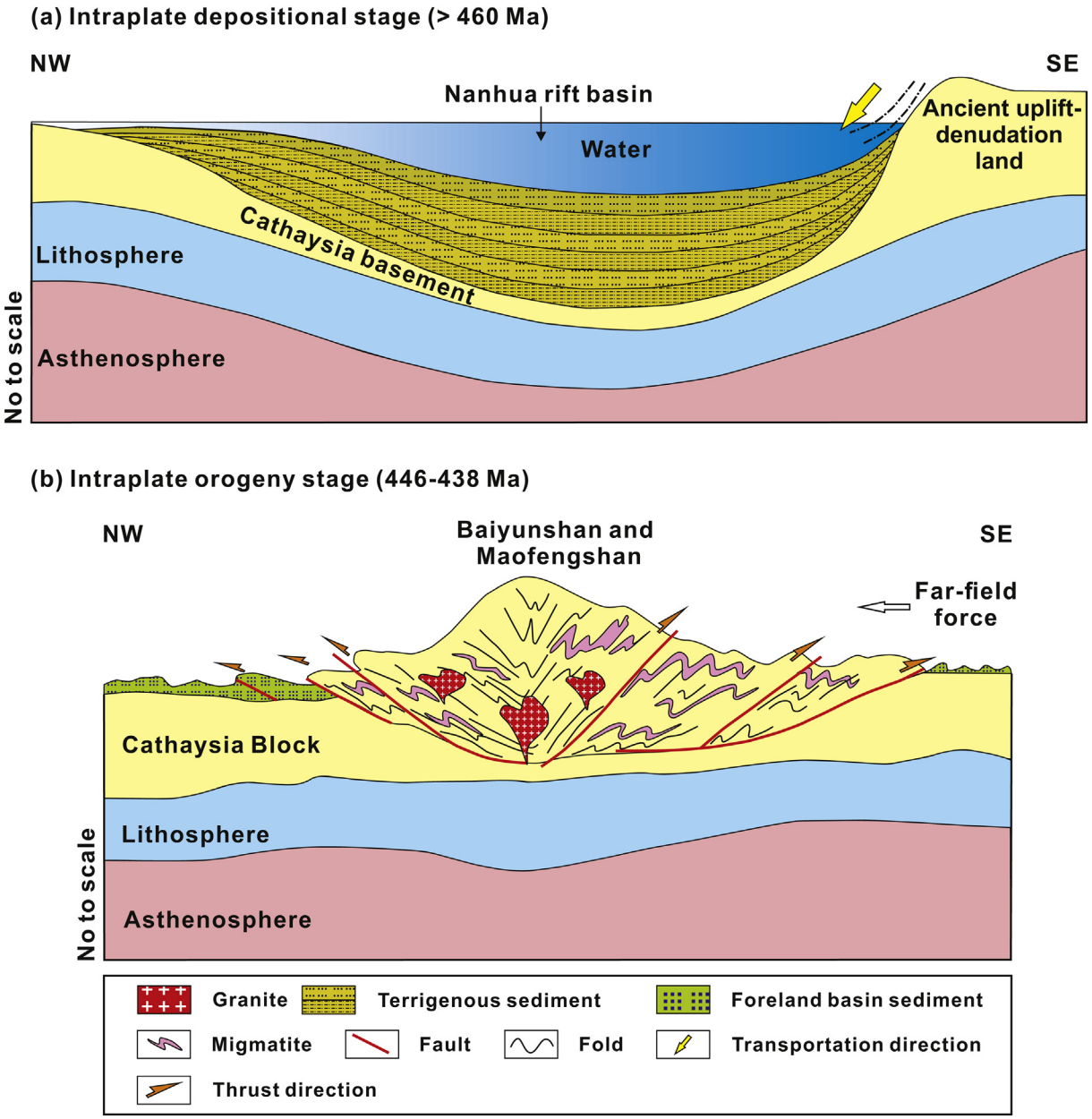

Fig. 8. Petrogenetic model for the Baiyunshan–Maofengshan granites (modified after Wang et al., 2013c; Shu et al., 2015). (a) The SCB underwent continental rifting during the Neoproterozoic, and the metasedimentary source rocks of the Baiyunshan–Maofengshan granites may have been deposited in the Neoproterozoic Nanhua rift basin. (b) During the early Paleozoic (446–438 Ma), far-field stresses possibly resulted from the amalgamation of the Australian Plate, Indian Plate, and SCB along the northern margin of east Gondwanaland, which resulted in intraplate subduction or overthrusting in the Baiyunshan–Maofengshan region. Intraplate subduction or overthrusting buried the terrigenous sediments to mid-crustal levels and the crust was further thickened. Heat generated by the decay of radioactive elements in the sedimentary rocks, and possible heating by mantle-derived mafic magmas in the adjacent region (not shown), induced dehydration partial melting of the metasedimentary rocks and subordinate amphibolites, which generated the Baiyunshan–Maofengshan granites in the Guangzhou region.

continental rifting during the Neoproterozoic (Wang et al., 2011a; Wang and Li, 2003), and the metasedimentary source rocks of the Baiyunshan–Maofengshan granites might have been deposited in the Neoproterozoic Nanhua rift basin (Wang and Li, 2003; Wang et al., 2011a; Fig. 8a). Subsequently, during the early Paleozoic (446–438 Ma), intraplate subduction or overthrusting buried these terrigenous sediments to mid-crustal levels and caused crustal thickening (Fig. 8b). Heat generated through the decay of radioactive elements in the sedimentary rocks (e.g., Li et al., 2010; Wang et al., 2007), possibly enhanced by heating from mantle-derived mafic magmas in the adjacent region (Xie et al., 2020; Xu and Xu, 2015), induced dehydration partial melting of the metasedimentary rocks and subordinate amphibolites, which generated the Baiyunshan–Maofengshan granites in the Guangzhou region (Fig. 8b). Geological, geochemical, geochronological, paleomagnetic, and paleontological evidence suggests that the SCB was located adjacent to the western Australian and northeastern Indian plates in east Gondwanaland during the early Paleozoic (Xu and Xu, 2015, and references therein; Wang et al., 2011b, and references therein). Therefore, the intracontinental orogeny might have formed due to far-field stresses induced by the amalgamation of the Australian Plate,

Indian Plate, and SCB along the northern margin of east Gondwanaland (Shu et al., 2015; Wang et al., 2010; Wang et al., 2011b).

5. Conclusions

(1) SIMS and LA–ICP–MS zircon U—Pb ages indicate that the biotite, two-mica, and muscovite granites in the Baiyunshan–Maofengshan area of Guangzhou, South China, were formed during the early Paleozoic (446–438 Ma).
(2) The Baiyunshan muscovite and two-mica granites were formed by partial melting of metasedimentary rocks, while the Maofengshan biotite granites were formed by partial melting of a hybridized crustal source containing metasedimentary rocks and subordinate amphibolites.
(3) The granites probably formed in an intracontinental orogenic setting.

Supplementary data to this article can be found online at https://doi.org/10.1016/j.lithos.2020.105763.

Declaration of Competing Interest

The authors declare that they have no known competing financial interests or personal relationships that could have appeared to influence the work reported in this paper.

Acknowledgements

We thank the Editor-in-Chief Michael Roden and two anonymous reviewers whose constructive criticisms and suggestions have improved this paper significantly. We appreciate the assistance of Lin-Li Chen, Xin-Yu Wang, Zong-Yong Yang, and Wan-Long Hu during the whole-rock and mineral major element analyses and zircon cathodoluminescence imaging. Xiang-Lin Tu, Sheng-Ling Sun, Wen Zeng, Le Zhang, Yue Qi, Wan-Long Hu, and Peng Sun are thanked for their help with the whole-rock trace element and Sr-Nd isotope and zircon Hf isotope analyses. We also thank Ya-Nan Yang, Qing Yang, Miao-Hong He, Bo-Qin Xiong, and Yue-Heng Yang for their assistance with SIMS and LA–ICP–MS zircon U—Pb dating and SIMS zircon O isotope analyses. Gong-Jian Tang and Wei Dan are thanked for their helpful suggestions and discussions. Financial support for this research was provided by the Key Program of Guangzhou City (No. 201707020032) and National Key R & D Program of China (No. 2016YFC0600407). This is contribution No.IS–2907 from GIGCAS.

References

Abdel Rahman, A.M., 1994. Nature of biotites from alkaline, calcalkaline, and peraluminous magmas. J. Petrol. 35, 525–541.
Anderson, J.L., 1996. Status of thermobarometry in granitic batholiths. Earth Environ. Sci. Trans. R. Soc. Edinb. 87, 125–138.
Bergemann, C.A., Jung, S., Berndt, J., Stracke, A., Hauff, F., 2014. Generation of magnesian, high-K alkali-calcic granites and granodiorites from amphibolitic continental crust in the Damara orogen, Namibia. Lithos 198-199, 217–233.
Cawood, P.A., Kröner, A., Collins, W.J., Kusky, T.M., Mooney, W.D., Windley, B.F., 2009. Accretionary orogens through Earth history. Geol. Soc. Lond. Spec. Publ. 318, 1–36.
Chen, J.F., Jahn, B.M., 1998. Crustal evolution of southeastern China: Nd and Sr isotopic evidence. Tectonophysics 284, 101–133.
Chen, X., Zhang, Y.D., Fan, J.X., Cheng, J.F., Li, Q.J., 2010. Ordovician graptolite-bearing strata in southern Jiangxi with a special reference to the Kwangsian orogeny. Sci. China Earth Sci. 53, 1602–1610.
Choukroune, P., 1992. Tectonic evolution of the Pyrenees. Annu. Rev. Earth Planet. Sci. 20, 143–158.
Copeland, P., Currie, C.A., Lawton, T.F., Murphy, M.A., 2017. Location, location, location: the variable lifespan of the Laramide orogeny. Geology 45, 223–226.
Dobosi, G., Kempton, P.D., Downes, H., Embey–Isztin, A., Thirlwall, M., Greenwood, P., 2003. Lower crustal granulite xenoliths from the Pannonian Basin, Hungary, part 2: Sr–Nd–Pb–Hf and O isotope evidence for formation of continental lower crust by tectonic emplacement of oceanic crust. Contrib. Mineral. Petrol. 144, 671–683.
Faure, M., Shu, L.S., Wang, B., Charvet, J., Choulet, F., Monié, P., 2009. Intracontinental subduction: a possible mechanism for the early Palaeozoic Orogen of SE China. Terra Nova 21, 360–368.
Feng, S.J., Zhao, K.D., Ling, H.F., Chen, P.R., Chen, W.F., Sun, T., Jiang, S.Y., Pu, W., 2014. Geochronology, elemental and Nd–Hf isotopic geochemistry of Devonian A-type granites in Central Jiangxi, South China: constraints on petrogenesis and post-collisional extension of the Wuyi–Yunkai orogeny. Lithos 206, 1–18.
Ferry, J.M., Watson, E.B., 2007. New thermodynamic models and revised calibrations for the Ti-in-zircon and Zr-in-rutile thermometers. Contrib. Mineral. Petrol. 154, 429–437.
Gao, P., Zhao, Z.F., Zheng, Y.F., 2014. Petrogenesis of Triassic granites from the Nanling Range in South China: implications for geochemical diversity in granites. Lithos 210-211, 40–56.
GDGBMR (Bureau of Geology and Mineral Resources of Guangdong Province), 1988. Regional Geology of Guangdong Province. Geological Publishing House, Beijing, p. 941.
Griffin, W.L., Pearson, N.J., Belousova, E., Jackson, S.E., Van Achterbergh, E., O'Reilly, S.Y., Shee, S.R., 2000. The Hf isotope composition of cratonic mantle: LAM-MC-ICPMS analysis of zircon megacrysts in kimberlites. Geochim. Cosmochim. Acta 64, 133–147.
Guan, Y.L., Yuan, C., Sun, M., Wilde, S., Long, X.P., Huang, X.L., Wang, Q., 2014. I-type granitoids in the eastern Yangtze Block: implications for the Early Paleozoic intracontinental orogeny in South China. Lithos 206, 34–51.
Guo, Z.F., Wilson, M., 2012. The Himalayan leucogranites: constraints on the nature of their crustal source region and geodynamic setting. Gondw. Res. 22, 360–376.
Hawkesworth, C.J., Turner, S.P., McDermott, F., Peate, D.W., Van Calsteren, P., 1997. U-Th isotopes in arc magmas: implications for element transfer from the subducted crust. Science 276, 551–555.
Hoskin, P., Black, L., 2000. Metamorphic zircon formation by solid-state recrystallization of protolith igneous zircon. J. Metam. Geol. 18, 423–439.
Huang, X.L., Yu, Y., Li, J., Tong, L.X., Chen, L.L., 2013. Geochronology and petrogenesis of the early Paleozoic I-type granite in the Taishan area, South China: middle-lower crustal melting during orogenic collapse. Lithos 177, 268–284.
Huang, H.Q., Li, X.H., Li, Z.X., Li, W.X., 2015. Formation of the Jurassic South China large Granitic Province: insights from the genesis of the Jiufeng pluton. Chem. Geol. 401, 43–58.
Jia, X.H., Wang, X.D., Yang, W.Q., 2017. Petrogenesis and geodynamic implications of the early Paleozoic potassic and ultrapotassic rocks in the South China Block. J. Asian Earth Sci. 135, 80–94.
Jiang, Y.H., Zhu, S.Q., 2017. Petrogenesis of the Late Jurassic peraluminous biotite granites and muscovite-bearing granites in SE China: geochronological, elemental and Sr–Nd–O–Hf isotopic constraints. Contrib. Mineral. Petrol. 172, 1–27.
Jiang, D.S., Xu, X.S., Xia, Y., Erdmann, S., 2018. Magma mixing in a granite and related rock association: insight from its mineralogical, petrochemical, and "reversed isotope" features. J. Geophys. Res. Solid Earth 123, 2262–2285.
Jung, S., Mezger, K., Hoernes, S., 1998. Petrology and geochemistry of syn- to post-collisional metaluminous A-type granites–a major and trace element and Nd-Sr-Pb-O-isotope study from the Proterozoic Damara Belt, Namibia. Lithos 45, 147–175.
Li, Z.X., Li, X.H., 2007. Formation of the 1300-km-wide intracontinental orogen and postorogenic magmatic province in Mesozoic South China: a flat-slab subduction model. Geology 35, 179–182.
Li, X.H., Wang, Y.X., Zhao, Z.H., Chen, D.F., Zhang, H., 1998. SHRIMP U-Pb zircon geochronology for amphibolite from the Precambrian basement in SW Zhejiang and NW Fujian Province. Geochimica 27, 327–334 (in Chinese with English abstract).
Li, X.H., Li, W.X., Wang, X.C., Li, Q.L., Liu, Y., Tang, G.Q., 2009. Role of mantle-derived magma in genesis of early Yanshanian granites in the Nanling Range, South China: in situ zircon Hf-O isotopic constraints. Sci. China Ser. D 52, 1262–1278.
Li, Z.X., Li, X.H., Wartho, J.A., Clark, C., Li, W.X., Zhang, C.L., Bao, C.M., 2010. Magmatic and metamorphic events during the early Paleozoic Wuyi-Yunkai orogeny, southeastern South China: new age constraints and pressure-temperature conditions. Geol. Soc. Am. Bull. 122, 772–793.
Li, X.H., Li, Z.X., Li, W.X., Wang, X.C., Gao, Y.Y., 2013. Revisiting the "C-type adakites" of the lower Yangtze River Belt, central eastern China: in-situ zircon Hf–O isotope and geochemical constraints. Chem. Geol. 345, 1–15.
Li, J.Y., Zhang, J., Zhao, X.X., Jiang, M., Li, Y.P., Zhu, Z.X., Feng, Q.W., Wang, L.J., Sun, G.H., Liu, J.F., Yang, T.N., 2016. Mantle subduction and uplift of intracontinental mountains: a case study from the Chinese Tianshan Mountains within Eurasia. Sci. Rep. 6, 1–8.
Li, J., Huang, X.L., Wei, G.J., Liu, Y., Ma, J.L., Han, L., He, P.L., 2018. Lithium isotope fractionation during magmatic differentiation and hydrothermal processes in rare-metal granites. Geochim. Cosmochim. Acta 240, 64–79.
Lin, S.F., Xing, G.F., Davis, D.W., Yin, C.Q., Wu, M.L., Li, L.M., Jiang, Y., Chen, Z.H., 2018a. Appalachian-style multi-terrane Wilson cycle model for the assembly of South China. Geology 46, 319–322.
Lin, S.F., Xing, G.F., Davis, D.W., Yin, C.Q., Wu, M.L., Li, L.M., Jiang, Y., Chen, Z.H., 2018b. Appalachian–style multi–terrane Wilson cycle model for the assembly of South China: REPLY. Geology 46, e447–e448.
Liu, X., Wang, Q., Ma, L., Yang, Z.Y., Hu, W.L., Ma, Y.M., Wang, J., Huang, T.Y., 2020. Petrogenesis of late Jurassic two-mica granites and associated diorites and syenite porphyries in Guangzhou, SE China. Lithos 364-365, 105537.
Ma, L., Wang, Q., Kerr, A.C., Yang, J.H., Xia, X.P., Ou, Q., Yang, Z.Y., Sun, P., 2017. Paleocene (ca. 62 Ma) leucogranites in southern Lhasa, Tibet: products of syn-collisional crustal anatexis during slab roll-back? J. Petrol. 58, 2089–2114.
Miller, C.F., Stoddard, E.F., Bradfish, L.J., Dollase, W.A., 1981. Composition of plutonic muscovite: genetic implications. Can. Mineral. 19, 25–34.
Morris, R.A., DeBari, S.M., Busby, C., Medynski, S., Jicha, B.R., 2019. Building arc crust: plutonic to volcanic connections in an extensional oceanic arc, the southern Alisitos arc, Baja California. J. Petrol. 60, 1195–1228.

Nex, P.A., Kinnaird, J.A., Oliver, G.J., 2001. Petrology, geochemistry and uranium mineralisation of post-collisional magmatism around Goanikontes, southern Central Zone, Damaran Orogen, Namibia. J. Afr. Earth Sci. 33, 481–502.
Osterhus, L., Jung, S., Berndt, J., Hauff, F., 2014. Geochronology, geochemistry and Nd, Sr and Pb isotopes of syn-orogenic granodiorites and granites (Damara orogen, Namibia) – arc-related plutonism or melting of mafic crustal sources? Lithos 200-201, 386–401.
Passarelli, C.R., Verma, S.K., Mcreath, I., Basei, M.A., Siga, O., 2019. Tracing the history from Rodinia break-up to the Gondwana amalgamation in the Embu Terrane, southern Ribeira Belt, Brazil. Lithos 342-343, 1–17.
Patiño Douce, A.E., 1999. What do experiments tell us about the relative contributions of crust and mantle to the origin of granitic magmas? Geol. Soc. Lond. Spec. Publ. 168, 55–75.
Patiño Douce, A.E., Harris, N., 1998. Experimental constraints on Himalayan anatexis. J. Petrol. 39, 689–710.
Pearce, J.A., 1996. Sources and settings of granitic rocks. Episodes 19, 120–125.
Pirajno, F., Ernst, R.E., Borisenko, A.S., Fedoseev, G., Naumov, E.A., 2009. Intraplate magmatism in Central Asia and China and associated metallogeny. Ore Geol. Rev. 35, 114–136.
Raimondo, T., Clark, C., Hand, M., Faure, K., 2011. Assessing the geochemical and tectonic impacts of fluid–rock interaction in mid-crustal shear zones: a case study from the intracontinental Alice Springs Orogen, Central Australia. J. Metam. Geol. 29, 821–850.
Scaillet, B., Pichavant, M., Roux, J., 1995. Experimental crystallization of leucogranite magmas. J. Petrol. 36, 663–705.
Shu, L.S., Wang, B., Cawood, P.A., Santosh, M., Xu, Z.Q., 2015. Early Paleozoic and Early Mesozoic intraplate tectonic and magmatic events in the Cathaysia Block, South China. Tectonics 34, 1600–1621.
Shu, L.S., Song, M.J., Yao, J.L., 2018. Appalachian-style multi-terrane Wilson cycle model for the assembly of South China: COMMENT. Geology 46, e445.
Smithies, R.H., Howard, H.M., Evins, P.M., Kirkland, C.L., Kelsey, D.E., Hand, M., Wingate, M.T.D., Collins, A.S., Belousova, E., 2011. High-temperature granite magmatism, crust–mantle interaction and the Mesoproterozoic intracontinental evolution of the Musgrave Province, Central Australia. J. Petrol. 52, 931–958.
Stammeier, J., Jung, S., Romer, R.L., Berndt, J., Garbe-schönberg, D., 2015. Petrology of ferroan alkali-calcic granites: synorogenic high-temperature melting of undepleted felsic lower crust (Damara orogen, Namibia). Lithos 224-225, 114–125.
Sun, S.-S., McDonough, W.F., 1989. Chemical and isotopic systematics of oceanic basalts: implications for mantle composition and processes. Geol. Soc. Lond. Spec. Publ. 42, 313–345.
Wang, J., Li, Z.X., 2003. History of Neoproterozoic rift basins in South China: implications for Rodinia break-up. Precambrian Res. 122, 141–158.
Wang, Q., Xu, J.F., Jian, P., Bao, Z.W., Zhao, Z.H., Li, C.F., Xiong, X.L., Ma, J.L., 2006. Petrogenesis of adakitic porphyries in an extensional tectonic setting, Dexing, South China: implications for the genesis of porphyry copper mineralization. J. Petrol. 47, 119–144.
Wang, Y.J., Fan, W.M., Sun, M., Liang, X.Q., Zhang, Y.H., Peng, T.P., 2007. Geochronological, geochemical and geothermal constraints on petrogenesis of the Indosinian peraluminous granites in the South China Block: a case study in the Hunan Province. Lithos 96, 475–502.
Wang, Y.J., Zhang, F.F., Fan, W.M., Zhang, G.W., Chen, S.Y., Cawood, P.A., Zhang, A.M., 2010. Tectonic setting of the South China Block in the early Paleozoic: resolving intracontinental and ocean closure models from detrital zircon U-Pb geochronology. Tectonics 29, 1–16.
Wang, X.C., Li, Z.X., Li, X.H., Li, Q.L., Zhang, Q.R., 2011a. Geochemical and Hf–Nd isotope data of Nanhua rift sedimentary and volcaniclastic rocks indicate a Neoproterozoic continental flood basalt provenance. Lithos 127, 427–440.
Wang, Y.J., Zhang, A.M., Fan, W.M., Zhao, G.C., Zhang, G.W., Zhang, Y.Z., Zhang, F.F., Li, S.Z., 2011b. Kwangsian crustal anatexis within the eastern South China Block: geochemical, zircon U-Pb geochronological and Hf isotopic fingerprints from the gneissoid granites of Wugong and Wuyi–Yunkai Domains. Lithos 127, 239–260.
Wang, Q., Chung, S.L., Li, X.H., Wyman, D.A., Li, Z.X., Sun, W.D., Qiu, H.N., Liu, Y.S., Zhu, Y.T., 2012. Crustal Melting and Flow beneath Northern Tibet: evidence from Mid-Miocene to Quaternary strongly Peraluminous Rhyolites in the Southern Kunlun Range. J. Petrol. 53, 2523–2566.
Wang, D., Zheng, J.P., Ma, Q., Griffin, W.L., Zhao, H., Wong, J., 2013a. Early Paleozoic crustal anatexis in the intraplate Wuyi–Yunkai orogen, South China. Lithos 175-176, 124–145.
Wang, Y.J., Fan, W.M., Zhang, G.W., Zhang, Y.H., 2013b. Phanerozoic tectonics of the South China Block: key observations and controversies. Gondw. Res. 23, 1273–1305.
Wang, Y.J., Zhang, A.M., Fan, W.M., Zhang, Y.H., Zhang, Y.Z., 2013c. Origin of paleosubduction-modified mantle for Silurian gabbro in the Cathaysia Block: geochronological and geochemical evidence. Lithos 160, 37–54.
Wang, Q., Hawkesworth, C.J., Wyman, D.A., Chung, S.L., Wu, F.Y., Li, X.H., Li, Z.X., Gou, G.N., Zhang, X.Z., Tang, G.J., Dan, W., Ma, L., Dong, Y.H., 2016. Pliocene-Quaternary crustal melting in central and northern Tibet and insights into crustal flow. Nat. Commun. 7, 1–11.
Wu, F.Y., Li, X.H., Zheng, Y.F., Gao, S., 2007. Lu-Hf isotopic systematics and their applications in petrology. Acta Petrol. Sin. 23, 185–220 (in Chinese with English abstract).
Xia, Y., Xu, X.S., Zou, H.B., Liu, L., 2014. Early Paleozoic crust–mantle interaction and lithosphere delamination in South China Block: evidence from geochronology, geochemistry, and Sr–Nd–Hf isotopes of granites. Lithos 184, 416–435.
Xie, Y.X., Ma, L.Y., Zhao, G.C., Xie, C.F., Han, Y.G., Li, J.H., Liu, Q., Yao, J.L., Zhang, Y.Y., Lu, Y.F., 2020. Origin of the Heping granodiorite pluton: implications for syn-convergent extension and asthenosphere upwelling accompanying the early Paleozoic orogeny in South China. Gondw. Res. 85, 149–168.
Xu, W.J., Xu, X.S., 2015. Early Paleozoic intracontinental felsic magmatism in the South China Block: petrogenesis and geodynamics. Lithos 234-235, 79–92.
Yang, D.S., Li, X.H., Li, W.X., Liang, X.Q., Long, W.G., Xiong, X.L., 2010. U–Pb and ^{40}Ar–^{39}Ar geochronology of the Baiyunshan gneiss (central Guangdong, south China): constraints on the timing of early Palaeozoic and Mesozoic tectonothermal events in the Wuyun (Wuyi-Yunkai) Orogen. Geol. Mag. 147, 481–496.
Yang, Z.Y., Wang, Q., Zhang, C.F., Yang, J.H., Ma, L., Wang, J., Sun, P., Qi, Y., 2019. Cretaceous (~ 100 Ma) high-silica granites in the Gajin area, Central Tibet: petrogenesis and implications for collision between the Lhasa and Qiangtang Terranes. Lithos 324, 402–417.
Yao, W.H., Li, Z.X., Li, W.X., Wang, X.C., Li, X.H., Yang, J.H., 2012. Post-kinematic lithospheric delamination of the Wuyi–Yunkai orogen in South China: evidence from ca. 435 Ma high-Mg basalts. Lithos 154, 115–129.
Yu, Y., Huang, X.L., He, P.L., Li, J., 2016. I-type granitoids associated with the early Paleozoic intracontinental orogenic collapse along pre-existing block boundary in South China. Lithos 248, 353–365.
Yu, P.P., Zhang, Y.Z., Zhou, Y.Z., Weinberg, R.F., Zheng, Y., Yang, W.B., 2019. Melt evolution of crustal anatexis recorded by the Early Paleozoic Baiyunshan migmatite-granite suite in South China. Lithos 332-333, 83–98.
Zhang, F.F., Wang, Y.J., Zhang, A.M., Fan, W.M., Zhang, Y.Z., Zi, J.W., 2012. Geochronological and geochemical constraints on the petrogenesis of Middle Paleozoic (Kwangsian) massive granites in the eastern South China Block. Lithos 150, 188–208.
Zhang, Q., Jiang, Y.H., Wang, G.C., Liu, Z., Ni, C.Y., Qing, L., 2015. Origin of Silurian gabbros and I-type granites in Central Fujian, SE China: implications for the evolution of the early Paleozoic orogen of South China. Lithos 216, 285–297.
Zhao, G.C., 2015. Jiangnan Orogen in South China: developing from divergent double subduction. Gondw. Res. 27, 1173–1180.
Zhao, L., Cui, X.H., Zhai, M.G., Zhou, X.W., Liu, B., 2019. Emplacement and metamorphism of the mafic rocks from the Chencai terrane within the Cathaysia Block: implications for the Paleozoic orogenesis of the South China Block. J. Asian Earth Sci. 173, 11–28.
Zhong, Y.F., Ma, C.Q., Liu, L., Zhao, J.H., Zheng, J.P., Nong, J.N., Zhang, Z.J., 2014. Ordovician appinites in the Wugongshan Domain of the Cathaysia Block, South China: geochronological and geochemical evidence for intrusion into a local extensional zone within an intracontinental regime. Lithos 198, 202–216.
Zhong, Y.F., Wang, L.X., Zhao, J.H., Liu, L., Ma, C.Q., Zheng, J.P., Zheng, Z.J., Luo, B.J., 2016. Partial melting of an ancient sub-continental lithospheric mantle in the early Paleozoic intracontinental regime and its contribution to petrogenesis of the coeval peraluminous granites in South China. Lithos 264, 224–238.
Zhou, X.M., Li, W.X., 2000. Origin of Late Mesozoic igneous rocks in Southeastern China: implications for lithosphere subduction and underplating of mafic magmas. Tectonophysics 326, 269–287.